Author/s:
Xu, W-L;Niu, M-S;Yang, X-Y;Bi, P-Q;Zhang, K-N;Xiong, C;Yuan, H-C;Smith, TA;Ghiggino, KP;Hao, X-T

Title:
Spatially Resolved Photophysical Dynamics in Perovskite Microplates Fabricated Using an Antisolvent Treatment

Date:
2017-11-30

Citation:
Xu, W. -L., Niu, M. -S., Yang, X. -Y., Bi, P. -Q., Zhang, K. -N., Xiong, C., Yuan, H. -C., Smith, T. A., Ghiggino, K. P. & Hao, X. -T. (2017). Spatially Resolved Photophysical Dynamics in Perovskite Microplates Fabricated Using an Antisolvent Treatment. The Journal of Physical Chemistry C, 121 (47), pp.26250-26255. https://doi.org/10.1021/acs.jpcc.7b09844.

Spatially Resolved Photophysical Dynamics in Perovskite Microplates Fabricated Using an Antisolvent Treatment

Wei-Long Xu,[†] Meng-Si Niu,[‡] Xiao-Yu Yang,[‡] Peng-Qing Bi,[‡] Kang-Ning Zhang,[‡] Chao Xiong,[†] Hong-Chun Yuan,[†] Trevor A. Smith,[§] Kenneth P. Ghiggino,[§] Xiao-Tao Hao [*,‡,§]

[†]School of Electrical and Photoelectronic Engineering, Changzhou Institute of Technology, Changzhou, Jiangsu 213002, China

[‡]School of Physics, State Key Laboratory of Crystal Materials, Shandong University, Jinan, Shandong 250100, China

[§]ARC Centre of Excellence in Exciton Science, School of Chemistry, The University of Melbourne, Parkville, Victoria 3010, Australia

Abstract: Perovskite microplates have important implications in the fields of functional electronics and optoelectronics. We report a facile strategy, antisolvent treatment for the growth of perovskite microplates. The morphology and crystalline quality of the microplates could be controlled by the amount of the chlorobenzene antisolvent used. An appropriate amount of antisolvent facilitates the formation of high quality perovskite microplates with no residual precursor remaining. Spatially and temporally resolved fluorescence measurements demonstrate the heterogeneity of defect state density and recombination processes in various perovskite microplate regions. The body center shows higher defect state density when compared with that in the edge or the corner of the microplate. Excessive antisolvent degrades the microplates into smaller particles. The results of this study reveal the factors that influence the crystallization process and photophysical dynamics of perovskite microplates.

[*]Corresponding author. E-mail: haoxt@sdu.edu.cn (X.T. Hao)

INTRODUCTION

Perovskite semiconductors have gained considerable attention due to their potential applications in optoelectronic devices including solar cells, light-emitting diodes, lasers and photodetectors.[1-10] Their promising device performance has been attributed to a range of attractive properties, such as high charge carrier mobility, intrinsic ambipolar character, large absorption coefficient, and low trap density.[2, 11-14] The morphology and quality of the active layer in perovskite devices are important parameters that determine the device performance.[9, 15, 16] Therefore, many methods, such as vacuum flash–assisted solution processing, solvent vapor annealing, interface engineering and antisolvent treatment are widely utilized to optimize the morphology and quality of the active layer.[15-18] Antisolvent treatment is a simple and effective technology that can be combined with the cost-effective solution fabrication method.[16] Wu et al.[15] reported that perovskite films show remarkable improvement in photoluminescence (PL) lifetime and surface coverage with antisolvent treatment, which leads to the improved efficiency and stability of perovskite light-emitting diodes. Cheng et al.[19] achieved the rapid and reproducible fabrication of high-quality perovskite thin films with antisolvent treatment. Shi et al.[11] found that perovskite single crystals with low trap-state density and long carrier diffusion could be produced by antisolvent vapor-assisted crystallization. Paek et al.[18] revealed that the addition of antisolvent has a substantial effect on the perovskite nucleation kinetics and device performance. In spite of these advances, there remain deficiencies in our understanding of how the antisolvent modifies the microstructure of perovskite films.

The effect of antisolvent on the photophysical processes in perovskite films is less well studied. Investigations are invariably focused on ensemble measurements that are averages over microscopically different areas.[20, 21] This restricts obtaining detailed information about material properties. Charge carrier dynamics in the sub-micron spatial region could be obtained by a combination of spatially and temporally resolved optical techniques.

Aside from polycrystalline thin films, microplates are another form of perovskite. Wang et al.[22] utilized perovskite microplates to create addressable photodetectors and well-performing field effect transistors with high field effect mobility. Whispering-gallery-mode microlasers have been achieved based on perovskite microplates.[23] In addition, the performance of photodetectors based on perovskite microplates have recently shown considerable improvement.[24] Perovskite microplates have been prepared by the methods of "liquid knife",[25] patterned growth of precursor microplate[22] or precipitation processes.[23] However, facile antisolvent treatment has been rarely explored to fabricate perovskite microplates.

In this work, chlorobenzene (CB) is chosen as the antisolvent because it is widely used to manipulate properties of perovskite films and therefore improve device performance.[16, 18, 19, 26, 27] A mixture of CB and N, N-dimethylformamide (DMF) in varied proportions is employed to study the antisolvent effect on the film morphology, crystal quality and photophysical dynamics. The crystalline qualities of perovskite films were measured by X-ray diffraction (XRD) and selected area electron diffraction (SAED). Time-resolved photoluminescence mapping was performed on

individual perovskite microplates to investigate the spatial distribution of photophysical dynamics.

EXPERIMENTAL SECTION

$PbBr_2$ and CH_3NH_3Br were supplied by Xi'an Polymer Light Technology Corp. DMF and CB were purchased from Aladdin. $PbBr_2$ (0.69g) and CH_3NH_3Br (0.21g) were separately dissolved in 5 ml DMF. The perovskite solution was prepared by mixing $PbBr_2$ and CH_3NH_3Br at the ratio of 1:1. The CB antisolvent is added into the perovskite solution with different DMF:CB volume ratios of 1:0, 1:1, 1:10 and 1:50 respectively. Other DMF:CB volume ratios, such as 1:5 and 1:100 are also investigated, and the results are shown in the Supporting Information. The blend solutions were aged overnight without stirring. The final samples were prepared by drop-casting the solutions onto glass substrates cleaned by sonication with acetone, alcohol, isopropanol respectively.

A Rigaku Ultima IV X-ray diffractometer was used to obtain the XRD results. A field emission scanning electron microscope (SEM, Zeiss-Sigma) equipped with an energy dispersive X-ray spectrometer (EDS, Oxford instruments) was used to measure the microstructure and the chemical element distribution of the perovskite films. Transmission electron microscopy (TEM) and SAED were carried out using a JEM2100, JEOL Ltd. instrument. Steady-state fluorescence spectra were measured using a spectrometer (PG2000 Pro, Ideaoptics Instruments Co., Ltd.) with an excitation wavelength of 400 nm. Fluorescence microscopy images were collected using an inverted fluorescence microscope (IX7392F, Olympus). Time-resolved PL

mapping was carried out with a confocal optical microscopy system (Nanofinder FLEX2, Tokyo Instrument Inc.) combined with a CCD (DU420A-OE, ANDOR) and time-correlated single photon counting (TCSPC) module (SPC-150, Becker & Hickl). Angle-resolved reflectance spectra were measured by an angle-resolved fiber optical spectrometer (R1 series, Ideaoptics Instruments Co., Ltd).

RESULTS AND DISCUSSION

The SEM images (Figure 1) demonstrate the obvious morphology differences between the perovskite films processed with different amounts of CB. Many small clusters are present that are connected with each other in the pristine perovskite film (Figure 1a). The clusters became larger when the solvent (DMF):antisolvent (CB) ratio is 1:1 (Figure 1b). The clusters become thoroughly separated and show the cuboid structure when the ratio increased to 1:10 (Figure 1c). This is related to the underlying mechanism of the antisolvent approach which speeds up nucleation via creation of local supersaturation with sufficient antisolvent treatment.[18] However, excessive CB degrades the regular perovskite microplates into small clusters, and the boundaries between the clusters became ambiguous, as shown in Figure 1d. This behavior may be caused by the differences in boiling point, miscibility and dielectric constants between the two solvents.[18] EDS mapping was used to study the chemical composition in the microplates. Figures 1(e-f) show the uniform distribution of Pb and Br in the microplates, and the ratio between Br and Pb is 29:11 (Figure S1), which is in good agreement with the stoichiometry in $CH_3NH_3PbBr_3$. This demonstrates that $PbBr_2$ and CH_3NH_3Pb have nearly reacted and with no residual

precursor remaining in the perovskite microplates.

The crystalline quality of the perovskite films was characterized by XRD, as shown in Figure 2a. The distinct diffraction peaks in the XRD patterns of perovskite films at 14.9°, 30°, 33.7° and 45.7° (corresponding to the (100), (200), (210) and (300) planes, respectively) indicate the high degree of cubic phase structure (space group $Pm\bar{3}m$)[5,11]. In the pristine perovskite film, diffraction peaks centered at 6° and 8° are ascribed to the precursors, which demonstrate that the reaction between CH_3NH_3Br and $PbBr_2$ is not complete.[28] This may be related to undesirable crystallization processes caused by the different solubility between the two precursors.[17] The crystalline quality of perovskite microplates was improved with the addition of CB evidenced by the increased intensity of perovskite crystalline peaks and decreased crystalline intensity of the precursors. This illustrates that CB facilitates the reaction between the two precursors. This is particularly the case when the ratio reaches 1:10, the crystalline quality of perovskite is optimal without any residual precursor being evident, inferring that the reaction between the two precursors is nearly complete. At the same time, the crystalline phase of the perovskite film is pure. However, the crystalline quality was poor in the perovskite film processed with a 1:50 solvent ratio, as observed by the decreased diffraction intensity of the (100) and (200) peaks and increased prominence of the precursor diffraction peaks. The main reason for this phenomenon is that antisolvent reduces the solubility of the precursors, leading to their reduced reaction.[19] TEM was used to further characterize the crystalline structure of a single perovskite microplate. A representative TEM image, shown in Figure 2b, is similar to the SEM

result. The circled region was selected for the SAED measurement, as shown in the inset of Figure 2b. Clear diffraction spots in the SAED image can be indexed to the tetragonal crystal structure of perovskite.[8] This indicates that the large-area perovskite microplate processed with 1:10 mixed solvent ratio was composed of a reasonably large single crystal.

Figure 3 shows the PL spectra of perovskite films processed with different amounts of CB. The PL spectra show an emission peak located at around 540 nm with a full width at half maximum (FWHM) of 25 nm, in good agreement with those of perovskite bulk films processed without antisolvent treatment.[20] A clear red-shift of the PL spectra is observed in the perovskite films processed with CB in comparison with the pristine film. This red-shift of the emission may be attributed to photon recycling, lattice strain and assorted changes at the grain boundaries.[15] Large grain size polycrystalline films exhibit the red-shifted PL peak compared to small polycrystalline ones.[29] Excessive CB treatment (1:50) causes an emission peak blue-shift relative to the 1:10 ratio spectrum, which suggests a decrease in crystalline domain size. This result is consistent with the XRD and SEM analyses.

Figure 4a depicts the fluorescence microscopy image of a perovskite film processed with 1:10 solvent ratio, and others are shown in Figure S4. It can be seen that all perovskite films emit green light under the blue light excitation (380 nm). Figure S4a shows the ‘snowflake’ structure of the pristine perovskite film. The ‘snowflake’ structure changes to the particle clusters in the perovskite film when the solvent ratio is 1:1. When the ratio is 1:10, microplates could be observed in the perovskite film.

The perovskite microplates were degraded into small particles in the perovskite films with 1:50 treatment. The microplates in Figure 4a demonstrate strong emission at the edge and much weaker emission in the body of the microplate. To further investigate the fluorescence dynamics of perovskite microplates, one typical microplate was selected on which two dimensional PL and time-resolved PL measurements were performed. The photophysical dynamics of perovskite films processed with different DMF:CB ratios were also measured and shown in Figure S5. The fluorescence intensity mapping (Figure 4b) shows a distinctly inhomogeneous distribution of fluorescence intensity. Three typical regions in the microplate - body center, the edge and the corner - are marked with A, B and C respectively. The fluorescence intensity is strong at the edge and corners of the perovskite microplate, and decreases gradually from the edge region to the body center. This is indicative of optical confinement within the perovskite microplate.[20] Figure 4c shows the fluorescence lifetime distribution over the perovskite microplate. Spatial inhomogeneities in the emission decay behavior are attributed to the positions exhibiting various crystalline quality, but these are unresolvable in the PL spectra that were recorded over the bulk region of the films. The integrated area under the fluorescence decay profile is proportional to the fluorescence intensity.[30] Figure 4d shows the fluorescence decay profiles corresponding to the three identified regions in the microplate. The decays are obviously not monoexponential, so multiexponential functions have been used to fit the decay profiles. The decay times, relative intensities and weighted-average lifetimes of three typical regions in the microplate are listed in Table 1. The

proportion of the short lifetime component is the highest, reaching 90.4%, in region A compared with that in region B and C. Stranks et al.[31] reported that electronic subgap trap states exist in the energy diagram of perovskites. The carriers in the excited state will transit to the trap states to fill the trap states first. A short emission lifetime has been associated with the faster nonradiative deactivation process as the carriers decay to the trap states.[20] From the percentage and value of the short lifetime, we speculate that the defect state density is high in the body center of the microplate. The long-lived fluorescence decay component has been attributed to the bimolecular recombination at the band edge between the electrons in the conduction band and the holes in the valence band[13, 20]. The smaller value and significantly lower percentage of τ_2 in position A when compared with that in positions B and C further supports the proposition of a higher defect density within the body of the microplates. The carrier recombination and lifetime are strongly dependent on the crystalline quality of the perovskite, which would be masked by the ensemble averaged decay process.[32-34] The recombination processes and defect state density in the different perovskite microplate regions can be clearly distinguished by the combination of temporally and spatially resolved optical measurements.

Angle-resolved reflection spectra were measured to study the optical reflection property of perovskite films, as shown in Figure 5. The reflected light intensity increases with increasing angle in the perovskite film processed with 1:10 solvent ratio, while other perovskite films do not show this trend (Figure S6). The increased reflectivity may derive from the scattering of light by regular microplates planes.[35]

The reflection peak changes little with the detection angle variation in the perovskite processed with 1:10 solvent ratio. This indicates that the colors of the perovskite films are nearly angle-independent. This distinct property of perovskite films may have important applications in microscopic color displays.[36]

CONCLUSIONS

In summary, we have successfully fabricated perovskite microplates using an antisolvent treatment. The amount of antisolvent has an important role in influencing and controlling the morphology and crystalline quality of perovskite microplates. Time-resolved PL mapping reveals the different recombination processes and defect state density in various regions of individual perovskite microplates, which would be overlooked in ensemble measurements. Two emission decay components from analysis of fluorescence decay profiles are attributed to the decay of excited carriers to defect states or the valence band. The results of this study provide a deeper understanding of the mechanism for antisolvent control of perovskite crystallization and highlight the heterogeneity of photophysical dynamics in single microplates.

Supporting Information

The distribution of characteristic element with the EDS measurement (Figure S1); SEM and XRD data of the perovskite films processed with a mixed solvent of DMF:CB with the ratios of 1:5 and 1:100 (Figure S2 and S3); fluorescence microscopy images of perovskite films (Figure S4); fluorescence lifetime images and fluorescence decay profiles (Figure S5); angle-resolved reflectance spectra (Figure S6).

Acknowledgements

This work was supported by the Natural Science Foundation of Jiangsu Higher Education (No.17KJB140001), the National Natural Science Foundation of China (No.11574181, 61631166001), Open Research Fund of State Key Laboratory Polymer Physics and Chemistry, Changchun Institute of Applied Chemistry, Chinese Academy of Sciences, Research project of "333 high-level talents training project" in Jiangsu Province of China (No. BRA2016111) and the Jiangsu Province Key R & D projects (No. BE2016200). We also acknowledge support by the International Research and Research Training Fund (IRRTF) from the University of Melbourne and the ARC Centre of Excellence in Exciton Science (CE170100026).

Figures and Figure Captions

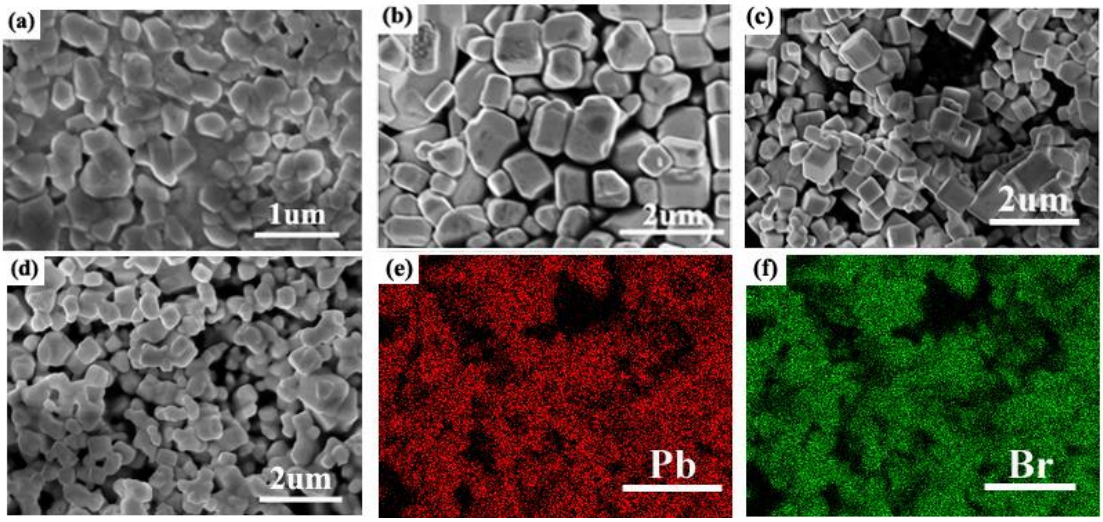

Figure 1. SEM images of perovskite films processed with a mixed solvent of DMF:CB with the ratio of (a) 1:0; (b) 1:1; (c) 1:10; (d) 1:50; (e-f) Pb and Br element mapping images corresponding to (c).

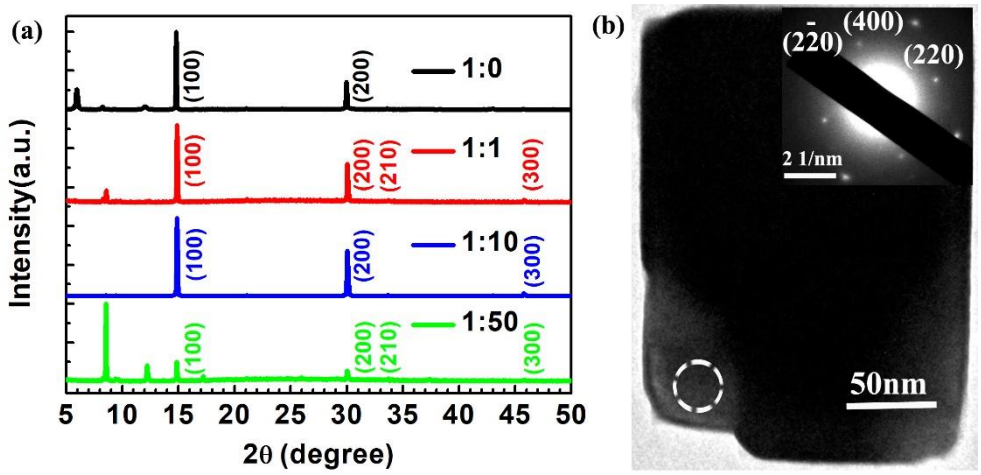

Figure 2. (a) XRD patterns of perovskite films processed with mixed solvent of DMF:CB with the ratios of 1:0, 1:1, 1:10 and 1:50; (b) TEM image of a single perovskite microplate. The inset is the corresponding SAED.

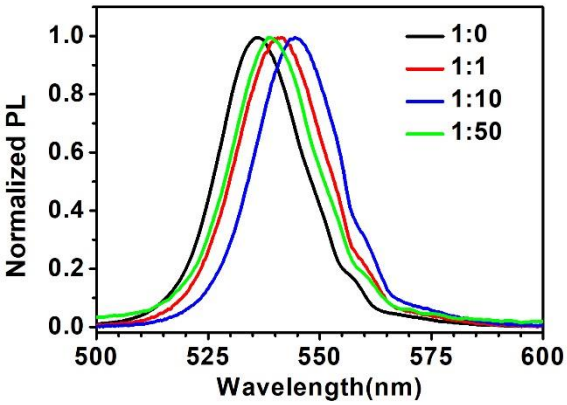

Figure 3. Normalized PL spectra of perovskite films processed with a mixed solvent of DMF:CB with the ratio of (a) 1:0; (b) 1:1; (c) 1:10; (d) 1:50.

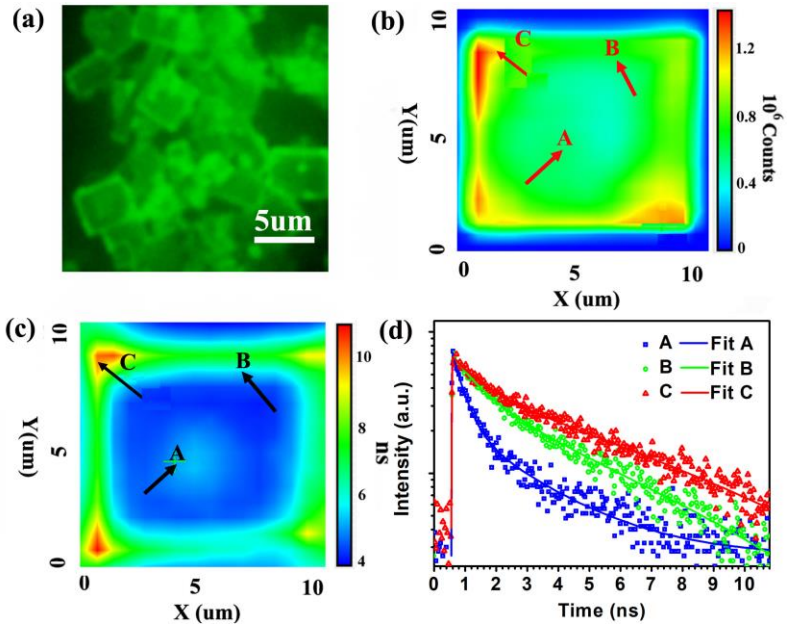

Figure 4. (a) Fluorescence microscopy images of perovskite films processed with a mixed solvent of DMF:CB with a ratio of 1:10; (b-c) fluorescence intensity and lifetime images for an individual perovskite microplate respectively, (d) fluorescence decay profiles recovered from the lifetime image.

Table 1. Fluorescence decay times, relative intensities and weighted-average lifetimes of three typical regions in the microplate

	A	B	C
τ_1	0.38 ns(90.4%)	0.87 ns(60.7%)	0.82 ns(51.2%)
τ_2	2.40 ns(9.6%)	4.43 ns(39.3%)	5.87 ns(48.8%)
τ_m	0.57 ns	2.27 ns	3.28 ns

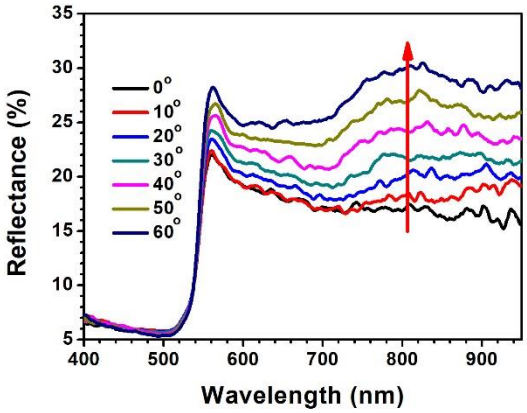

Figure 5. Angle-resolved reflectance spectra of perovskite films processed with a mixed solvent of DMF:CB with the ratio of 1:10. The detection angle varies from 0°to 60°with 10°increments.

References

1. Zhang, Q.; Su, R.; Liu, X.; Xing, J.; Sum, T. C.; Xiong, Q., High-Quality Whispering-Gallery-Mode Lasing from Cesium Lead Halide Perovskite Nanoplatelets. *Adv. Funct. Mater.*, 2016, **26**, 6238-6245.
2. Saliba, M.; Wood, S. M.; Patel, J. B.; Nayak, P. K.; Huang, J.; Alexander-Webber, J. A.; Wenger, B.; Stranks, S. D.; Hoerantner, M. T.; Wang, J. T.-W.; et al. Structured Organic-Inorganic Perovskite Toward a Distributed Feedback Laser. *Adv. Mater.*, 2016, **28**, 923-929.
3. Fu, Y.; Zhu, H.; Schrader, A. W.; Liang, D.; Ding, Q.; Joshi, P.; Hwang, L.; Zhu, X. Y.; Jin, S., Nanowire Lasers of Formamidinium Lead Halide Perovskites and Their Stabilized Alloys with Improved Stability. *Nano Lett.*, 2016, **16**, 1000-1008.
4. Adinolfi, V.; Ouellette, O.; Saidaminov, M. I.; Walters, G.; Abdelhady, A. L.; Bakr, O. M.; Sargent, E. H., Fast and Sensitive Solution-Processed Visible-Blind Perovskite UV Photodetectors. *Adv. Mater.*, 2016, **28**, 7264-7268.
5. Zhu, H.; Fu, Y.; Meng, F.; Wu, X.; Gong, Z.; Ding, Q.; Gustafsson, M. V.; Trinh, M. T.; Jin, S.; Zhu, X. Y., Lead Halide Perovskite Nanowire Lasers with Low Lasing Thresholds and High Quality Factors. *Nat. Mater.*, 2015, **14**, 636-642.
6. Chen, W.; Wu, Y.; Yue, Y.; Liu, J.; Zhang, W.; Yang, X.; Chen, H.; Bi, E.; Ashraful, I.; Graetzel, M.; et al. Efficient and Stable Large-Area Perovskite Solar Cells with Inorganic Charge Extraction Layers. *Science*, 2015, **350**, 944-948.
7. Tan, Z.-K.; Moghaddam, R. S.; Lai, M. L.; Docampo, P.; Higler, R.; Deschler, F.; Price, M.; Sadhanala, A.; Pazos, L. M.; Credgington, D.; et al. Bright Light-Emitting Diodes Based on Organometal Halide Perovskite. *Nat. Nanotechnology*, 2014, **9**, 687-692.
8. Wang, W.; Ma, Y.; Qi, L., High-Performance Photodetectors Based on Organometal Halide Perovskite Nanonets. *Adv. Funct. Mater.*, 2017, **27**, 1603653.
9. Li, X.; Bi, D.; Yi, C.; Décoppet, J. D.; Luo, J.; Zakeeruddin, S. M.; Hagfeldt, A.; Grätzel, M., A Vacuum Flash-Assisted Solution Process for High-Efficiency Large-Area Perovskite Solar Cells. *Science*, 2016, **353**, 58.
10. Xu, W. L.; Niu, M. S.; Yang, X. Y.; Yuan, H. C.; Xiong, C.; Zhu, X. F.; Hao, X. T., Aqueous Self-Assembled Perovskite Microfibers for Sensitive Photodetectors. *Org. Electronics*, 2017, **48**, 106-111.
11. Shi, D.; Adinolfi, V.; Comin, R.; Yuan, M. J.; Alarousu, E.; Buin, A.; Chen, Y.; Hoogland, S.; Rothenberger, A.; Katsiev, K.; et al. Low Trap-State Density and Long Carrier Diffusion in Organolead Trihalide Perovskite Single Crystals. *Science*, 2015, **347**, 519-522.
12. Dong, Q. F.; Fang, Y. J.; Shao, Y. C.; Mulligan, P.; Qiu, J.; Cao, L.; Huang, J. S., Electron-Hole Diffusion Lengths > 175μm in Solution-Grown $CH_3NH_3PbI_3$ Single Crystals. *Science*, 2015, **347**, 967-970.
13. Manser, J. S.; Kamat, P. V., Band Filling with Free Charge Carriers in Organometal Halide Perovskites. *Nat. Photonics*, 2014, **8**, 737-743.
14. Stranks, S. D.; Eperon, G. E.; Grancini, G.; Menelaou, C.; Alcocer, M. J. P.; Leijtens, T.; Herz, L. M.; Petrozza, A.; Snaith, H. J., Electron-Hole Diffusion Lengths Exceeding 1 Micrometer in an Organometal Trihalide Perovskite Absorber. *Science*, 2013, **342**, 341-344.
15. Wu, C.; Zou, Y.; Wu, T.; Ban, M.; Pecunia, V.; Han, Y.; Liu, Q.; Song, T.; Duhm, S.; Sun, B., Improved Performance and Stability of All-Inorganic Perovskite Light-Emitting Diodes by Antisolvent Vapor Treatment. *Adv. Funct. Mater.*, 2017, **27**, 1700338.

16. Ummadisingu, A.; Steier, L.; Seo, J. Y.; Matsui, T.; Abate, A.; Tress, W.; Grätzel, M., The Effect of Illumination on the Formation of Metal Halide Perovskite Films. *Nature*, 2017, **545**, 208-212.
17. Yu, Y.; Yang, S.; Lei, L.; Cao, Q.; Shao, J.; Zhang, S.; Liu, Y., Ultrasmooth Perovskite Film via Mixed Anti-Solvent Strategy with Improved Efficiency. *Acs Appl. Mater. Interfaces*, 2017, **9**, 3667-3676.
18. Paek, S.; Schouwink, P.; Athanasopoulou, E. N.; Cho, K.; Grancini, G.; Lee, Y.; Zhang, Y.; Stellacci, F.; Nazeeruddin, M. K.; Gao, P., From Nano-to Micrometer Scale: The Role of Antisolvent Treatment on High Performance Perovskite Solar Cells. *Chem. Mater.*, 2017, **29**, 3490-3498.
19. Xiao, M.; Huang, F.; Huang, W.; Dkhissi, Y.; Zhu, Y.; Etheridge, J.; Grayweale, A.; Bach, U.; Cheng, Y. B.; Spiccia, L., A Fast Deposition-Crystallization Procedure for Highly Efficient Lead Iodide Perovskite Thin-Film Solar Cells. *Angew. Chem. Int. Ed.*, 2014, **53**, 9898-9903.
20. Liao, Q.; Hu, K.; Zhang, H. H.; Wang, X. D.; Yao, J. N.; Fu, H. B., Perovskite Microdisk Microlasers Self-Assembled from Solution. *Adv. Mater.*, 2015, **27**, 3405-3410.
21. Xing, J.; Liu, X. F.; Zhang, Q.; Ha, S. T.; Yuan, Y. W.; Shen, C.; Sum, T. C.; Xiong, Q., Vapor Phase Synthesis of Organometal Halide Perovskite Nanowires for Tunable Room-Temperature Nanolasers. *Nano Lett.*, 2015, **15**, 4571-4577.
22. Wang, G.; Li, D.; Cheng, H. C.; Li, Y.; Chen, C. Y.; Yin, A.; Zhao, Z.; Lin, Z.; Wu, H.; He, Q., Wafer-scale Growth of Large Arrays of Perovskite Microplate Crystals for Functional Electronics and Optoelectronics. *Science Advances*, 2015, **1**, e1500613.
23. Gao, Y.; Wang, S.; Huang, C.; Yi, N.; Wang, K.; Xiao, S.; Song, Q., Room Temperature Three-Photon Pumped $CH_3NH_3PbBr_3$ Perovskite Microlasers. *Sci. Rep.*, 2017, **7**, 45391.
24. Yi, N.; Wang, S.; Duan, Z.; Wang, K.; Song, Q.; Xiao, S., Tailoring the Performances of Lead Halide Perovskite Devices with Electron-Beam Irradiation. *Adv. Mater.*, 2017, **29**, 1701636.
25. Feng, J.; Yan, X.; Zhang, Y.; Wang, X.; Wu, Y.; Su, B.; Fu, H.; Jiang, L., "Liquid Knife" to Fabricate Patterning Single-Crystalline Perovskite Microplates toward High-Performance Laser Arrays. *Adv. Mater.*, 2016, **28**, 3732.
26. Ngo, T. T.; Suarez, I.; Antonicelli, G.; Cortizolacalle, D.; Martinezpastor, J. P.; Mateoalonso, A.; Morasero, I., Enhancement of the Performance of Perovskite Solar Cells, LEDs, and Optical Amplifiers by Anti-Solvent Additive Deposition. *Adv. Mater.*, 2017, **29**, 1604056.
27. Zheng, X.; Chen, B.; Wu, C.; Priya, S., Room Temperature Fabrication of $CH_3NH_3PbBr_3$ by Anti-Solvent Assisted Crystallization Approach for Perovskite Solar Cells with Fast Response and Small J-V Hysteresis. *Nano Energy*, 2015, **17**, 269-278.
28. Fang, X.; Zhang, K.; Li, Y.; Yao, L.; Zhang, Y.; Wang, Y.; Zhai, W.; Tao, L.; Du, H.; Ran, G., Effect of Excess $PbBr_2$ on Photoluminescence Spectra of $CH_3NH_3PbBr_3$ Perovskite Particles at Room Temperature. *Appl. Phys. Lett.*, 2016, **108**, 071109.
29. Wu, B.; Nguyen, H. T.; Ku, Z.; Han, G.; Giovanni, D.; Mathews, N.; Fan, H. J.; Sum, T. C., Discerning the Surface and Bulk Recombination Kinetics of Organic–Inorganic Halide Perovskite Single Crystals. *Adv. Energy Mater.*, 2016, **6**, 1600551.
30. Smith, T. A.; Ghiggino, K. P., A Review of the Analysis of Complex Time-Resolved Fluorescence Anisotropy Data. *Methods Appl. Fluoresc.*, 2015, **3**, 022001.
31. Stranks, S. D.; Burlakov, V. M.; Leijtens, T.; Ball, J. M.; Goriely, A.; Snaith, H. J., Recombination Kinetics in Organic-Inorganic Perovskites: Excitons, Free Charge, and Subgap States. *Phys. Review Appl.*, 2014, **2**, 034007.

32. Guo, Z.; Manser, J. S.; Wan, Y.; Kamat, P. V.; Huang, L., Spatial and Temporal Imaging of Long-Range Charge Transport in Perovskite Thin Films by Ultrafast Microscopy. *Nat. Commun.*, 2015, **6**, 7471.

33. Hao, X.-T.; McKimmie, L. J.; Smith, T. A., Spatial Fluorescence Inhomogeneities in Light-Emitting Conjugated Polymer Films. *J. Phys. Chem. Lett.*, 2011, **2**, 1520-1525.

34. Simpson, M. J.; Doughty, B.; Yang, B.; Xiao, K.; Ma, Y.-Z., Spatial Localization of Excitons and Charge Carriers in Hybrid Perovskite Thin Films. *J. Phys. Chem. Lett.*, 2015, **6**, 3041-3047.

35. Qin, M.; Huang, Y.; Li, Y.; Su, M.; Chen, B.; Sun, H.; Yong, P.; Ye, C.; Li, F.; Song, Y., A Rainbow Structural-Color Chip for Multisaccharide Recognition. *Angew. Chem. Int. Ed.*, 2016, **128**, 7025-7028.

36. Zhang, Y.; Dong, B.; Chen, A.; Liu, X.; Shi, L.; Zi, J., Using Cuttlefish Ink as an Additive to Produce Non-Iridescent Structural Colors of High Color Visibility. *Adv. Mater.*, 2015, **27**, 4719-4724.

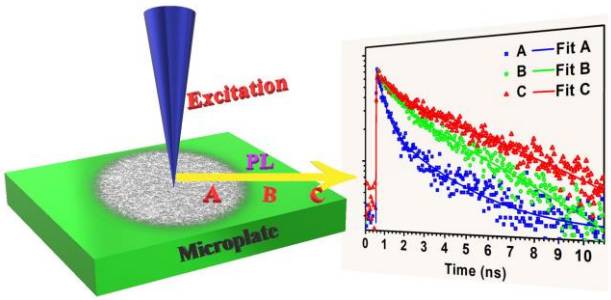
Excitation
PL
A
B
C
Microplate
A
B
C
Fit A
Fit B
Fit C
0 1 2 3 4 5 6 7 8 9 10
Time (ns)

TOC Graphic